Available online at www.sciencedirect.com
ScienceDirect
Journal of Sound and Vibration 323 (2009) 864–876
JOURNAL OF SOUND AND VIBRATION
www.elsevier.com/locate/jsvi

Energy criterion for potential well escapes in a bistable magnetic pendulum

B.P. Mann

Department of Mechanical Engineering and Material Science, Duke University, Durham, NC 27708, USA

Received 23 July 2008; received in revised form 19 December 2008; accepted 8 January 2009
Handling Editor: S. Bolton
Available online 20 February 2009

Abstract

This paper examines the dynamic behavior of a bistable experiment comprised a pendulum and two magnets. Investigations focus on determining when the oscillations about one equilibrium will overcome an adjacent potential barrier and escape to a neighboring attractor. Studies identify the parameters of the experimental system before investigating the generalization of an escape criterion. A specific outcome is the generalization of an energy-based criterion that can be used to predict escapes for forced and/or parametrically excited systems.

1. Introduction

The escape from a potential well is a problem of universal importance in the physical sciences [1]. In fact, a great number of dynamical systems can be characterized by their likelihood to overcome an adjacent potential barrier and escape to a neighboring attractor. As an example, consider the following highly disparate application areas where recent works take aim at understanding the jump response of a Duffing oscillator, the capsizing of naval vessels, the snap-through buckling of arches, and the bistable regions encountered in atomic force microscopy [1–5]. Since this abrupt jump in the state of the system can sometimes trigger a catastrophic event, it becomes necessary to understand the escape phenomenon and establish a criterion to predict when an escape is likely to occur.

Several researchers have investigated escape problems for systems with quadratic and cubic nonlinearities [1,2,5–7]. The escape problem complexity has also prompted investigations of basins of attraction metamorphoses [8,9] and indeterminate bifurcation phenomena [10,11]. In addition to these studies of forced systems, the presence of indeterminate bifurcations has been discovered in parametrically excited systems [12]. For clarification purposes, we note that parametrically excited systems contain a periodic coefficient in the governing equation. Related to these past studies is a criterion examined in Ref. [7] for inevitable quasi-steady escapes. While this work examined the period-one motion of an externally forced oscillator, the escape criterion has not been investigated for a parametrically excited system. Thus the above prior works serve as the motivation for the present study where the escape behavior is examined for a parametrically excited system.

E-mail address: brian.mann@duke.edu

0022-460X/$ - see front matter © 2009 Elsevier Ltd. All rights reserved.
doi:10.1016/j.jsv.2009.01.012

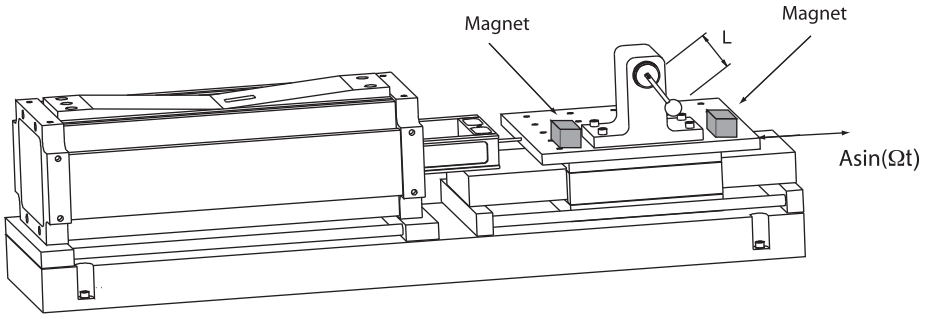

Fig. 1. Schematic diagram of the experimental system with removable magnets to allow for separate characterization of the pendulum and magnetic forces.

Outside of the present application, parametrically excited systems have been studied extensively in the literature (e.g. see Refs. [13–15]). Some of the methods available for stability analysis are Hill's method [14,15], Floquet theory [16–22], and perturbation techniques [15]. In contrast, the present work differs due to the focus on an energy-based criterion to investigate the loss of stability. More specifically, the interest is in using the energy criterion to determine when a potential well escape will occur.

This paper investigates a threshold criterion for escapes observed in a parametrically excited system. The system of interest is a magnetic pendulum subjected to a uniform gravitational field and highly nonlinear magnetic forces. Asymmetric potential wells are created due to subtle imperfections caused by differences in the strength of each magnet and imperfections in the relative locations of the magnets with respect to a ferromagnetic pendulum (see Fig. 1). Numerical and experimental investigations are performed to study nonlinear behavior of the system. Quasi-steady escapes are then examined for the forced system under the variation of a single control parameter.

The remaining content of this paper is organized as follows. The next section describes the experimental apparatus. This is followed by a section that derives the governing equation of motion. The fourth section describes the experimental parameter identification efforts used to characterize the system's parameters. The bifurcation behavior and the basins of attraction are then studied for the unforced system. The fifth section examines quasi-steady escapes for the parametrically excited system with forcing. We then discuss the necessary changes to an escape criterion, described in Ref. [7], to account for the escapes observed in the experimental system.

2. Description of the experimental apparatus

A schematic drawing of the experimental system is shown in Fig. 1. Measurements of the pendulum angular oscillations were obtained by supplying a constant voltage to a Novatechnik,[1] model P2200, low-torque potentiometer and recording the time-varying voltage drop provided by the potentiometer internal resistor. Apart from being a low-torque device, an additional unique feature of this potentiometer was an internal conductive plastic track which provides a uniformly scaled analog voltage (i.e. this feature differs from the typical wire-wound potentiometer that gives a step change in the voltage). The potentiometer was housed in a rigid base fixture and connected to a ferromagnetic, 75 mm long, threaded rod that was inserted into a 19 mm diameter stainless steel sphere. The mass of the assembled pendulum sphere and rod was measured to be $m = 35$ g. The pendulum base fixture was fabricated from aluminum and mounted onto the air bearing shake table that was connected to an APS Dynamics model 113 shaker (see Fig. 1). Attractive magnetic forces were created by introducing two neodymium magnets, grade N38, that were mounted on a flat plate that was constructed to have indexable features. The purpose of the indexing features was to provide very repeatable positioning of the magnets which were removed and replaced during the parameter identification process.

[1]Commercial equipment is identified for completeness and does not necessarily imply endorsement by the author.

3. Mathematical model

This section derives a math model for the angular oscillations of the horizontally shaken magnetic pendulum. Fig. 1 shows a pendulum whose pivot point is shaken in the horizontal direction with a sinusoidal motion of amplitude A and frequency Ω. The experimental system contains both gravitational and magnetic-restoring forces which results in the following expression for the potential energy:

$$U(\theta) = mgL(1-\cos\theta) + U_m(\theta), \tag{1}$$

where m is the pendulum mass, g is the gravitational constant, L is the pendulum effective length, $U_m(\theta)$ is the potential energy associated with the magnets, and θ is the angular displacement with reference to the downward position. An effective length variable, which identifies the position of the center of mass along the pendulum length, is used in place of the actual pendulum length to account for the distributed mass along the pendulum rod and attached spherical ball.

The functional form for the potential energy of the magnet is expressed as a polynomial series,

$$U_m(\theta) = \frac{\hat{\alpha}_1}{2}\theta^2 + \frac{\hat{\alpha}_2}{3}\theta^3 + \frac{\hat{\alpha}_3}{4}\theta^4, \tag{2}$$

where the coefficients $\hat{\alpha}_{1-3}$ capture the restoring force of the magnets. The kinetic energy of the system is given by

$$T = \tfrac{1}{2}m[(A\Omega\cos\Omega t + L\dot{\theta}\cos\theta)^2 + (L\dot{\theta}\sin\theta)^2]. \tag{3}$$

The governing equation for the system can be obtained by inserting Eqs. (1) and (3) into Lagrange's equation, which results in

$$\ddot{\theta} + \frac{c}{mL^2}\dot{\theta} - \frac{A\Omega^2}{L}\sin\Omega t\cos\theta + \frac{g}{L}\sin\theta + \frac{1}{mL^2}\frac{\partial U_m}{\partial\theta} = 0, \tag{4}$$

where c is a linear damping coefficient used to capture the velocity-dependent viscous and magnetic forces; the nonlinear restoring force of the magnets is given by $\partial U_m/\partial\theta$. At this point, it is worth highlighting the fact that terms of the order $\mathcal{O}(\theta^4)$ and higher have been neglected in the potential energy expression of Eq. (2) but not uniformly in the other terms of Eq. (4). While one could question whether the higher order terms are necessary to accurately capture the magnetic-restoring force, this consideration is answered in Section 4.2. Foreshadowing the results of that section, the approximation defined by Eq. (2) is assumed to be sufficient. After implementing a consistent level of approximation in Eq. (4), where $\sin\theta \approx \theta - \frac{1}{6}\theta^3$ and $\cos\theta \approx 1 - \frac{1}{2}\theta^2$, the governing equation can be written as

$$\ddot{\theta} + 2\zeta\omega\dot{\theta} + \omega^2\theta + \gamma(\sin\Omega t)\theta^2 + \beta\theta^3 + \sum_{n=1}^{3}\alpha_n\theta^n = 2\gamma\sin\Omega t, \tag{5}$$

where the constants ζ, ω, and γ can be expressed in terms of the previously defined variables as

$$\zeta = \frac{c}{2\omega mL^2}, \tag{6a}$$

$$\omega = \sqrt{\frac{g}{L}}, \tag{6b}$$

$$\gamma = \frac{A\Omega^2}{2L}, \tag{6c}$$

$$\beta = -\frac{\omega^2}{6}, \tag{6d}$$

$$\alpha_n = \frac{\hat{\alpha}_n}{mL^2}. \tag{6e}$$

It is interesting to note that Eq. (5) contains both parametric excitation and external forcing.

4. Experimental characterization and unforced oscillations

This section describes the experimental and analytical efforts undertaken to identify the magnetic pendulum model parameters. From the onset of this experiment, it was believed that characterizing the magnetic forces could be particularly challenging. Hence, the experimental system was built to allow independent characterization of the magnetic forces and pendulum model parameters. An interesting and unexpected outcome from this approach was that substantial velocity-dependent effects were observed from the magnets. Upon further investigation, the author realized that the rate-dependent forces were due to current damping, demagnetization effects, and the results of Lenz's Law (i.e. force is proportional to the time rate of change of the magnetic field) [23].

The remaining content for this section divides the parameter identification process into two distinct stages: (1) the unforced pendulum oscillations, in the absence of the magnetic forces, are studied to obtain model parameters for the pendulum (i.e. the effective length and mechanical damping); and (2) the fully assembled system is studied to provide independent characterization of the magnetic forces.

4.1. Identification of pendulum parameters from unforced oscillations

Under the assumption that the magnetic forces have been removed and that the pendulum is unforced (i.e. $\gamma = 0$ for the unforced system), the pendulum's angular oscillations are governed by the following equation of motion:

$$\ddot{\theta} + 2\mu\omega\dot{\theta} + \omega^2\theta + \beta\theta^3 = 0, \tag{7}$$

where the parameter μ is used to describe the mechanical damping in the absence of magnetic forces. This equation can be rewritten in a more convenient form for analysis,

$$\ddot{\theta} + \omega^2\theta = -f(\theta, \dot{\theta}), \tag{8}$$

where $f(\theta, \dot{\theta}) = 2\mu\omega\dot{\theta} + \beta\theta^3$. Following Ref. [15], the method of averaging is applied by assuming a solution of the form $\theta(t) = a\cos(\omega t + \phi) = a\cos\psi$, where $\psi = \omega t + \phi$. This will result in the following expressions for the slow variations of a and ϕ:

$$\dot{a} = \frac{1}{2\pi\omega}\int_0^{2\pi} (\sin\psi) f(a\cos\psi, -a\omega\sin\psi)\,\mathrm{d}\psi = -\mu\omega a, \tag{9a}$$

$$\dot{\phi} = \frac{1}{2\pi\omega a}\int_0^{2\pi} (\cos\psi) f(a\cos\psi, -a\omega\sin\psi)\,\mathrm{d}\psi = \frac{3a^2\beta}{8\omega}. \tag{9b}$$

After substituting $\beta = -\omega^2/6$, the amplitude and phase relationships become

$$a = a_0 \mathrm{e}^{-\mu\omega t}, \tag{10a}$$

$$\phi = \frac{a_0^2}{32\zeta}(\mathrm{e}^{-2\mu\omega t} - 1) + \phi_0, \tag{10b}$$

where a_0 and ϕ_0 are constants of integration. If the system is started from rest with an initial angular displacement of ϑ_0, the resulting transient solution becomes

$$\theta(t) = \vartheta_0 \mathrm{e}^{-\mu\omega t}\cos\left(\omega t + \frac{\vartheta_0^2}{32\mu}(\mathrm{e}^{-2\mu\omega t} - 1)\right), \tag{11}$$

which is in agreement with the approximate analytical solution obtained using the method of multiple scales (see Ref. [24]). Five independent free-fall oscillation tests were used for parameter estimation; these tests were anti-alias filtered at 20 Hz with a Stanford Research Systems, model SR640, low-pass filter and recorded at a sample rate of 300 Hz for 10-s time intervals. Using various different start angles, the estimated parameters were averaged over the total number of records to minimize the influence of experimental noise. Fig. 2 shows a comparison time series for the fitted parameters and the measured experimental test. It is noted that the experimental and theoretical results are in good agreement—thus illustrating the accuracy of the estimated parameters. The estimated parameters for the system were a damping ratio of $\mu = 0.0018$ and an effective length of $L = 0.0719$ m.

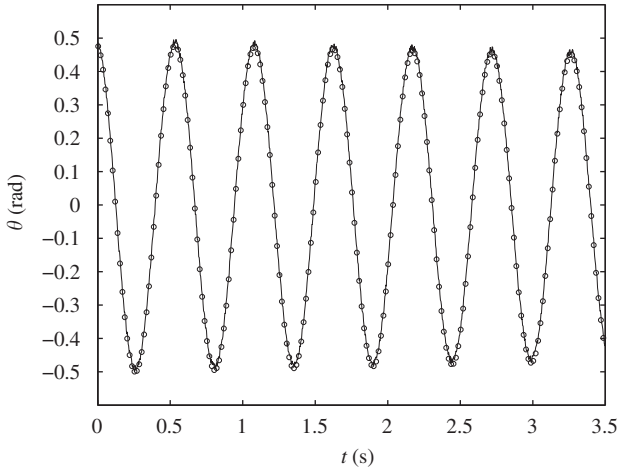

Fig. 2. Example overlay of the experimental data (○) onto the approximate analytical solution (solid line) for the identified pendulum parameters $\mu = 0.0018$ and $L = 0.0719$ (m).

4.2. Parametric identification of magnetic potentials

The introduction of the two neodymium magnets alters the potential energy of the system and redefines the basins of attraction. In particular, multiple stable equilibria solutions were observed during the unforced experimental trials. During these experiments, several start angles were used to investigate the multiple final equilibrium positions that were observed to be strongly dependent on subtle changes in the initial conditions—a hallmark of nonlinear systems. Fig. 3 shows two experimental trials that each reveal a different fixed point attractor.

The energy balance approach of Ref. [25] was used to identify the parameters for the magnetic pendulum. In an effort to remain brief, we describe only the salient features of this approach. The parameter identification scheme uses an energy balance between any two times, t_1 and t_2, which can be expressed as

$$T_{12} + U_{12} = -W_D, \tag{12}$$

where T_{12} is the change in kinetic energy, U_{12} is the change in potential energy, and W_D is the work due to energy dissipation over the time interval from t_1 to t_2. A matrix equation was then formed from Eq. (12) by balancing the energy over multiple time intervals. Angular velocity measurements were estimated from the measured angular position using cubic smoothing splines to avoid noise amplification in the signal derivatives [25–27]. Using more time intervals than the number of unknowns provides enough equations to determine the system parameters.

The above procedure was applied to 12 experimental trials to estimate the damping and magnetic-restoring forces. In an effort to check whether the potential energy expressions should contain terms higher than $\mathcal{O}(\theta^4)$, which is the assumed level of accuracy in the presented approach, magnetic forces were also characterized by expanding their potential energy expressions up to $\mathcal{O}(\theta^6)$. The results of Fig. 4a present a comparison graph for these two experimentally identified potential wells. Relatively speaking, both potential energy curves are comparable, with the largest differences at higher angular displacements. Therefore, it was decided to use the $\mathcal{O}(\theta^4)$ results since comparable levels of accuracy were obtained (see zoom of these results in Fig. 4b).

Table 1 provides a list of all the estimated model parameters. One parameter of particular interest is the damping coefficient, c, which captures the rate-dependent forces for the entire system. Estimating the equivalent damping ratio from Eq. (6a), where $\zeta = 0.0513$, reveals that 97% of the damping was due to the presence of the magnets.

5. Bifurcations and basins of attraction for the unforced system

During the unforced experimental trials, it was noticed that subtle changes in the pendulum release position would result in a different final equilibrium. In an effort to study this experimental observation, basins of

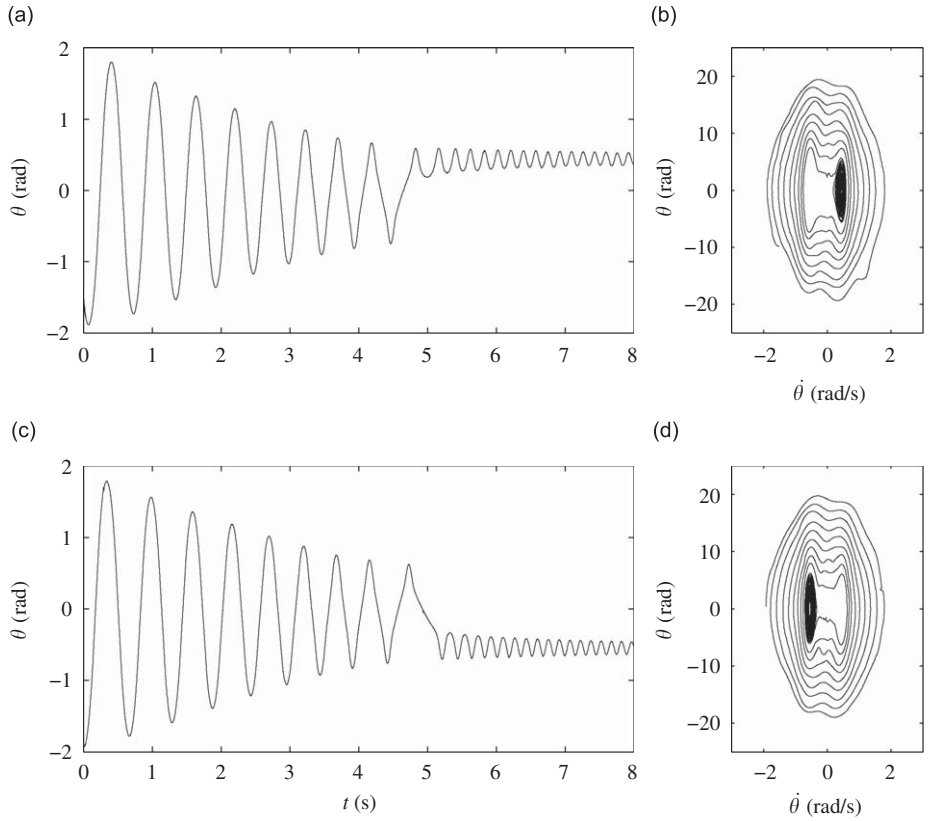

Fig. 3. Each row shows an experimental time history and the phase plane for a single experimental trial. Time histories are shown in graphs (a) and (c) and phase plane results are shown in graphs (b) and (d). The estimated velocity state was obtained by the application of cubic smoothing splines (as in Ref. [25]).

attraction were constructed with numerical simulation. Fig. 5 shows the basins of attraction, generated from Eq. (4), for a grid of initial conditions. For the angular velocities queried, this diagram confirms the experimental observation that the final state of the system is highly dependent upon the initial angular displacement. However, this is only true for start angles far enough away from the equilibria since start angles close to the equilibria remain trapped within the associated potential well.

The bifurcation behavior of the unforced system was also studied. Specifically, the pendulum's mass was used as the control parameter since this could be varied rather easily in the experimental system. The unforced equations are obtained by setting $\gamma = 0$ in Eq. (5). This gives the following first-order equation:

$$\dot{x}_1 = x_2, \tag{13a}$$

$$\dot{x}_2 = -2\zeta\omega x_2 - (\omega^2 + \alpha_1)x_1 - \alpha_2 x_1^2 - \left(\alpha_3 - \frac{\omega^2}{6}\right)x_1^3, \tag{13b}$$

where $x_1 = \theta$ and $x_2 = \dot{\theta}$. The equation above contains three equilibria located at $x_{2e} = 0$. The corresponding x_1 locations for each equilibria are

$$x_{1e} = 0, \tag{14a}$$

$$x_{1e} = \frac{-3\alpha_2 \pm 3\sqrt{\alpha_2^2 - \frac{2}{3}(6\alpha_3 - \omega^2)(\alpha_1 + \omega^2)}}{6\alpha_3 - \omega^2}. \tag{14b}$$

where a subscript has been added to each state variable to denote the equilibrium location (e.g. the equilibrium for x_1 has been written as x_{1e}). Fig. 6 shows a series of experimental measurements overlaid onto a theoretical

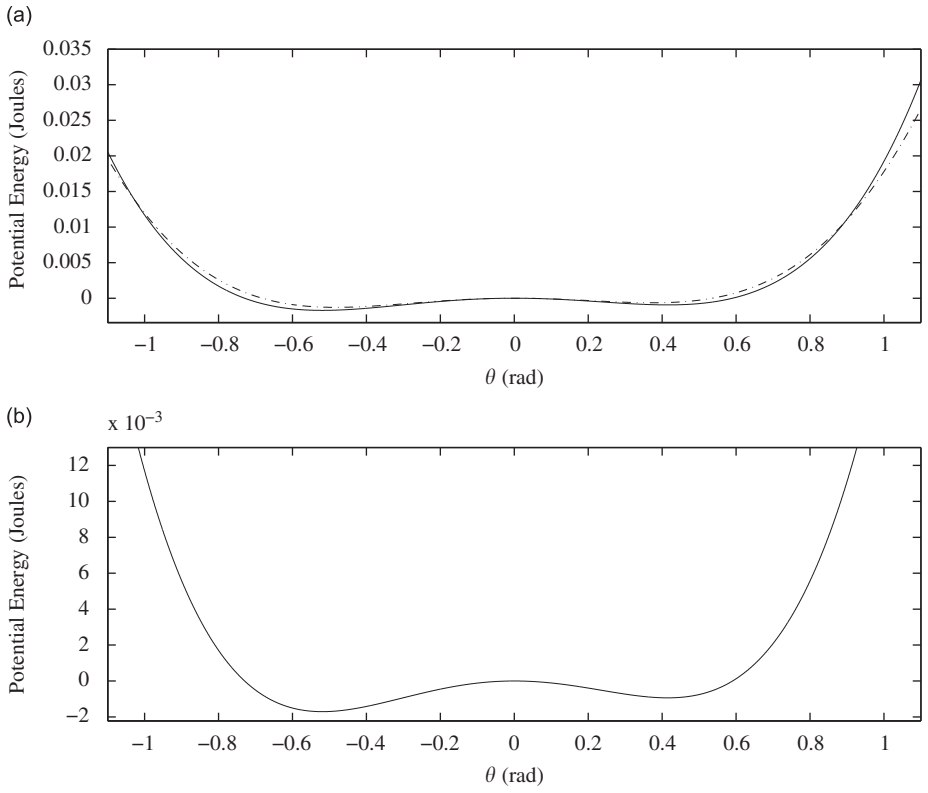

Fig. 4. Experimentally identified potential energy wells. Graph (a) shows energy well results when potential energy terms on the order of $\mathcal{O}(\theta^6)$ (dotted line) and $\mathcal{O}(\theta^4)$ (solid line) are retained in the analyses. Graph (b) is a zoom of the $\mathcal{O}(\theta^4)$ energy well, with local minima at $\theta \approx 0.415$ and -0.520 rad, that is used throughout the rest of this paper.

Table 1
Estimated system parameters.

Symbol	Value
m	0.035 kg
L	0.0719 m
c	2.17×10^{-4} N m s
$\hat{\alpha}_1$	-0.0481 N m/rad
$\hat{\alpha}_2$	0.0113 N m/rad^2
$\hat{\alpha}_3$	0.1125 N m/rad^3

bifurcation diagram. Although the mass does not explicitly appear in Eq. (14b), a different mass does result in different α_n values—as defined by Eq. (6e). Overall, the experimental measurements show relatively good agreement with the equilibria predicted by the theoretical model.

6. Escapes in the parametrically excited magnetic pendulum

The experimentally identified energy wells of Fig. 4b provide local minima at $\theta \approx 0.415$ rad and $\theta \approx -0.520$ rad. This section investigates potential well escapes when the system is initialized at one of these equilibria and then the oscillation amplitude of an electromagnetic shaker is slowly increased. While almost linear behavior is observed for relatively small shaker amplitudes, highly nonlinear behavior is observed as the shaker amplitude is increased. In particular, a sequence of period-doubling bifurcations is shown to trigger a potential well escape that eventually leads to chaos.

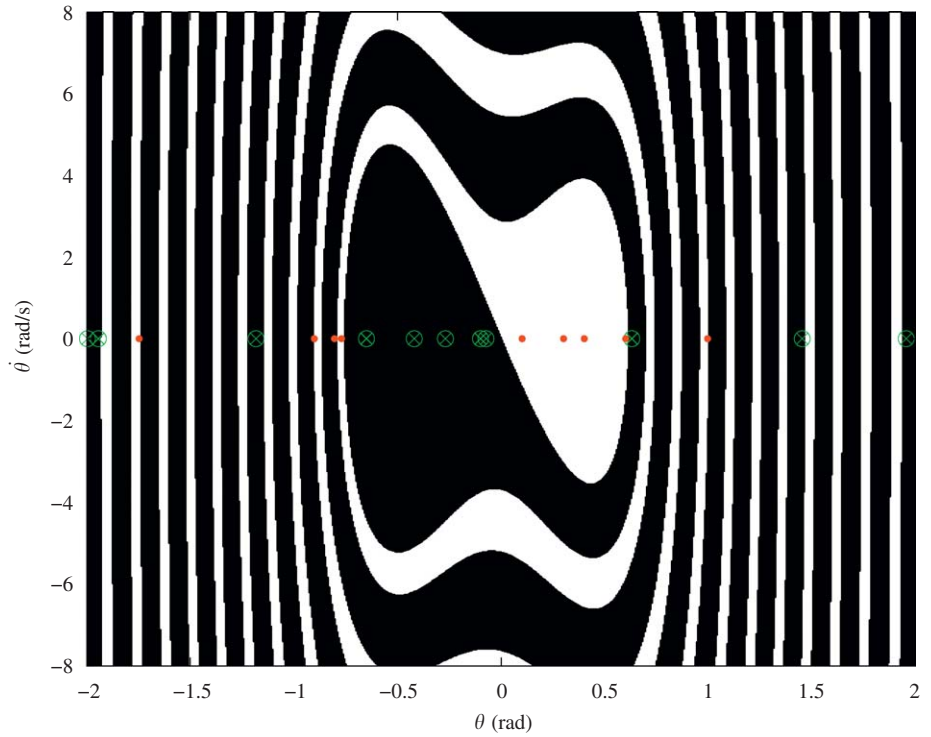

Fig. 5. Unforced basins of attraction with shaded regions showing the initial conditions where the motion came to rest at $\theta \approx -0.520$ rad and unshaded regions showing the initial conditions where the motion came to rest at $\theta \approx 0.415$ rad. A 300×600 grid of initial conditions was used to construct this graph. Markers are used to designate the experimental initial conditions with final angles of $\theta \approx 0.415$ rad (red •) and $\theta \approx -0.520$ rad (green ⊗). (For interpretation of the references to color in this figure legend, the reader is referred to the web version of this article.)

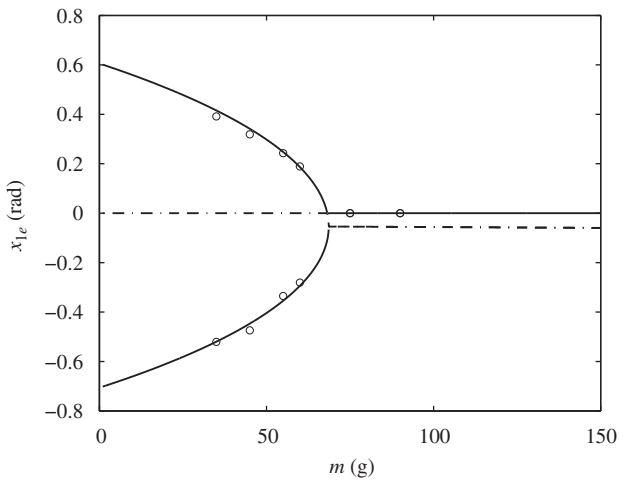

Fig. 6. Bifurcation diagram showing the stability of the static equilibria, x_{1e}, as a function of the pendulum mass. The solid line denotes the stable equilibria and the dashed line denotes an unstable equilibria. Experimental measurements, marked with a ○, indicate relatively good agreement.

This section investigates modifying an escape criterion from prior work [7]. Specifically, we have directly applied this criterion, but were unable to obtain accurate escape predictions. Our focus then shifted to modifying this criterion to accurately determine the escape threshold for a parametrically excited system. Our

results indicate that it is critical to include both the subharmonic response and the parametric excitation terms in the energy calculations to determine the threshold for quasi-steady escapes.

6.1. Periodic and subharmonic motions within each well

The experimental procedure consisted of initializing the magnetic pendulum at one of the unforced equilibrium conditions and then applying parametric excitation. The excitation frequency was held at a constant 5 Hz, $\Omega = 10\pi$ rad/s, and the imposed shaker amplitude was gradually increased until an escape occurred. For relatively low shaker amplitudes, periodic motions were observed within each well. Graphs (a) and (b) of Fig. 7 provide representative experimental and numerical results of a periodic attractor.

The motion complexity was observed to increase for larger shaker amplitudes. As an example, Fig. 7e gives a representative time history for an escape that was measured during experimentation. In this graph, subharmonic oscillations, within the well at $\theta \approx 0.415$ rad, are observed to escape and become trapped in the well centered at $\theta \approx -0.52$ rad. This abrupt transition in the system behavior is observed to occur for $\gamma \approx 45\,(\mathrm{rad/s})^2$. From the results presented in Fig. 8a, which are further described in the latter part of this section, the γ-value for an escape is shown to be premature. However, this premature escape behavior can be explained by the fact that the system becomes very sensitive to the rate of increase in the shaker amplitude. To elaborate, experimentally capturing the true bifurcation behavior requires quasi-static variation of the control parameter as opposed to the discrete adjustments that were used in the experimentation. However, further experimentation showed the result of Fig. 7e was a transient escape which often occurs prior to a quasi-steady escape.

An interesting observation, one that is not obvious from Fig. 7, is that period-doubling bifurcations were observed for subtle increases in the shaker amplitude. This experimental result was investigated numerically

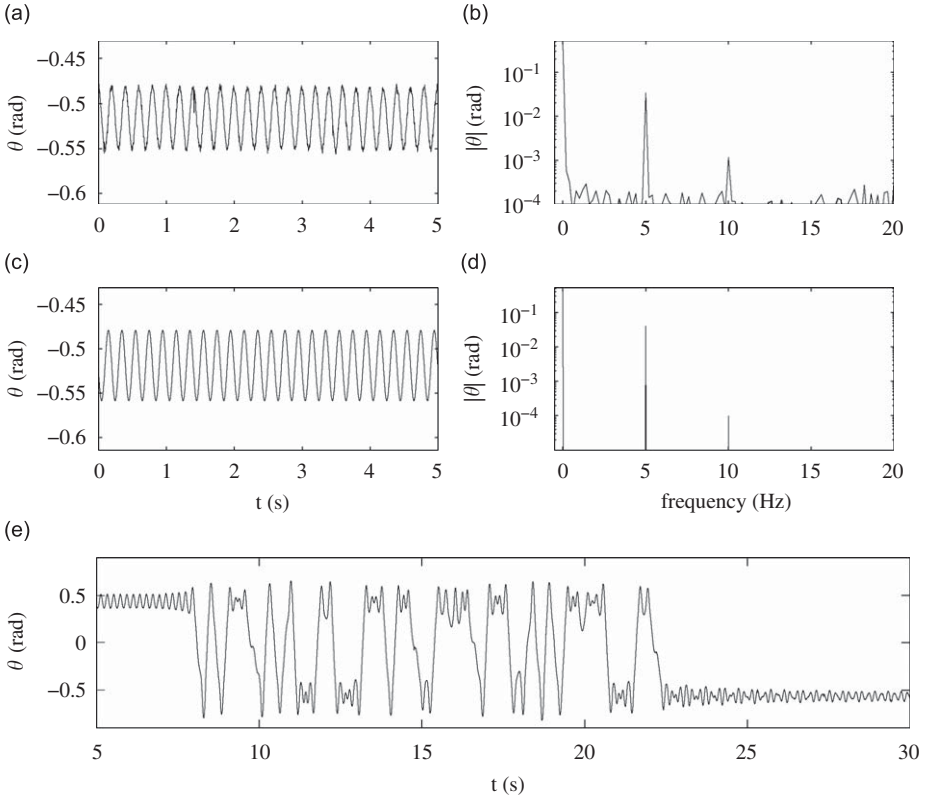

Fig. 7. Experimental time series and frequency spectrum, shown in (a) and (b), are compared to the numerical predictions of graphs (c) and (d) for $\gamma = 32\,(\mathrm{rad/s})^2$. Graph (e) shows an experimental example of a potential well escape due to a slow increase in the shaker amplitude or γ.

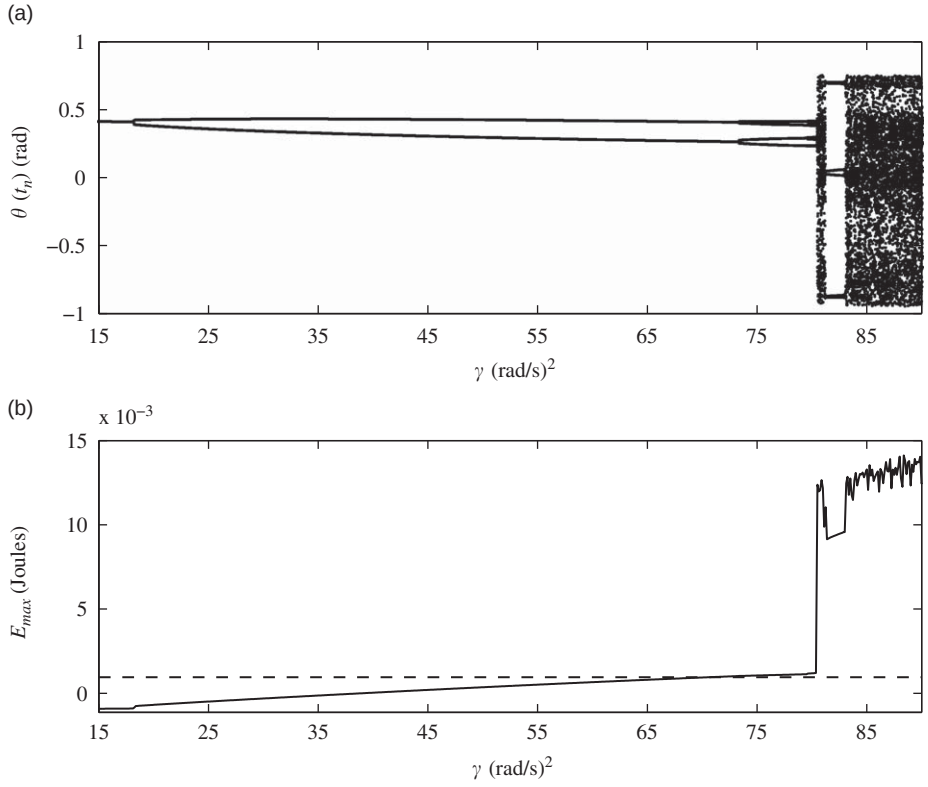

Fig. 8. Numerically generated angular position data sampled once per forcing period. Results are for the oscillations initiated within the well with a local minimum at $\theta_e = 0.415$ rad (shown in (a)). The solid line of (b) indicates the computed $E_{\max}(\theta, \dot{\theta})$ for the specified γ value. The dotted line represents the threshold value $U_b(\theta_e, \theta_u)$ where $\theta_u = 0$.

and is substantiated with the bifurcation diagram of Fig. 8. This graph shows a sequence of period-doubling bifurcations that are interrupted by a potential well escape triggered near $\gamma \approx 81\,(\mathrm{rad/s})^2$. Post-escape oscillations exhibit chaotic behavior prior to a region of period 6 behavior and chaos.

Since this type of abrupt jump in the state of the system can often trigger a catastrophic event, as in the capsize of a naval vessel, it is essential to develop a criterion that quantifies the threshold for such an escape. Recognizing this goal, the threshold criterion of Ref. [7] has been augmented to account for the subharmonic response of the parametrically excited system.

The procedure used to determine an escape under quasi-steady conditions is as follows: (1) the closest stable, θ_e, and unstable equilibrium, θ_u, are identified for the unforced system; (2) the location of the unstable equilibrium is then used to determine the energy required, $U_b(\theta_e, \theta_u) = U(\theta_u) - U(\theta_e)$, to overcome the potential energy barrier; (3) the response amplitude and phase relationships, whether determined analytically or with numerical simulation, are then used to calculate the maximum energy level, $E_{\max}(\theta, \dot{\theta}) = T(\dot{\theta}) + U(\theta)$, of the steady-state oscillation. With regards to the length of time to calculate $E_{\max}(\theta, \dot{\theta})$, the longest period in the predicted motion should be applied. A quasi-steady escape is predicted when the maximum energy of the steady-state oscillations rises to the level required to overcome the adjacent potential barrier, $E_{\max}(\theta, \dot{\theta}) \geqslant U_b(\theta_e, \theta_u)$. The primary difference between this criterion and the one from prior works is the consideration of response behavior that includes the subharmonic, harmonic, or chaotic behavior of the system. Furthermore, the parametric excitation term must be included in the calculation of the kinetic energy to obtain $E_{\max}(\theta, \dot{\theta})$.

Validation results for this threshold criterion are shown in Figs. 8b and 9b. For instance, Fig. 8b shows the $E_{\max}$ as a function of γ for the same data used to construct the stroboscopic samples of the angular displacement shown in Fig. 8a. For the results of Fig. 8b, a potential well escape is shown to occur once the value of $E_{\max}$ reaches the threshold criterion $U_b = 9.43 \times 10^{-4}$ J which occurs near $\gamma = 80.5\,(\mathrm{rad/s})^2$. It is also

evident that the sequence of period-doubling bifurcations is interrupted due to the escape. In this diagram, the value of $E_{\max}(\theta,\dot{\theta})$ was computed over 10 periods of the forced oscillations. The procedure for the numerical simulations required slowly and continuously varying the value of γ to ensure the presence of steady-state oscillations. Since γ was slowly varied, a constant value was assumed for each reported value of $E_{\max}(\theta,\dot{\theta})$.

When the oscillations originate in the neighboring well, as shown in Fig. 9, the same process is followed for computing $E_{\max}(\theta,\dot{\theta})$ and $U_b = 1.71\times10^{-3}$ J. As in the previous case, good agreement is obtained between the proposed threshold criterion and the escape that occurs near $\gamma = 48.5\,(\mathrm{rad/s})^2$. A counter-intuitive result can be observed when comparing Figs. 8b and 9b. In particular, the energy level for an escape to occur is much higher for the results of Fig. 9b, but an escape is triggered for a much smaller value of γ. However, this result is correctly predicted by the proposed threshold criterion and can be explained by the earlier onset of period doubling.

6.2. Post-escape oscillations

The periodically sampled time histories of Figs. 8 and 9 both show a series of period-doubling bifurcations that eventually lead to chaotic motion. This same behavior was also observed experimentally and the sample results from three experimental trials are shown in Fig. 10. These graphs show a 40 s snapshot of the recorded 300 s time history along with the corresponding Poincaré section. Since only angular displacements were recorded, visualization of the qualitative features of each chaotic attractor required the application of delayed embedding techniques to reconstruct a topologically equivalent phase space in angular displacement $\theta(t_n)$ vs. delayed angular displacement $\theta(t_n+\Delta t)$ coordinates. Following the methods suggested in Ref. [28], algorithms were developed to graph the mutual information function for the time series and the same time series shifted by Δt. The first minimum of the mutual information graph was used as the time shift, or delay, between the original time series and the $\theta(t+\Delta t)$ time series that are presented in Fig. 10.

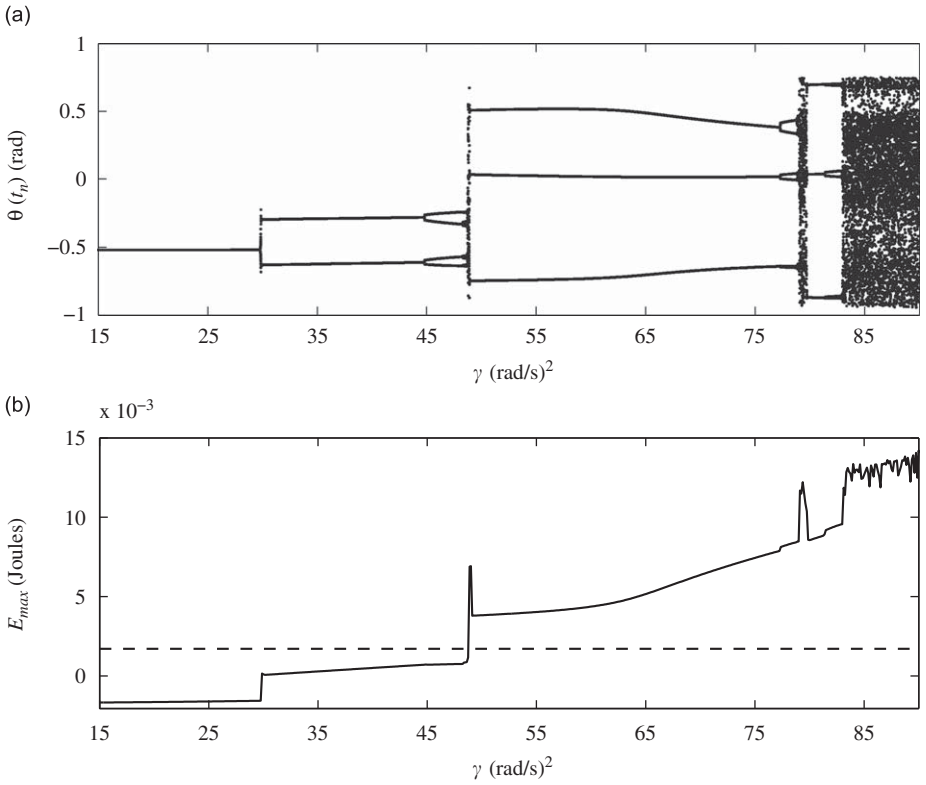

Fig. 9. Numerically generated angular position data sampled once per forcing period. Results are for the oscillations initiated within the well with a local minimum at $\theta_e = -0.520$ rad (shown in (a)). The solid line of (b) indicates the computed $E_{\max}(\theta,\dot{\theta})$ for the specified γ value. The dotted line represents the threshold value $U_b(\theta_e,\theta_u)$ where $\theta_u = 0$.

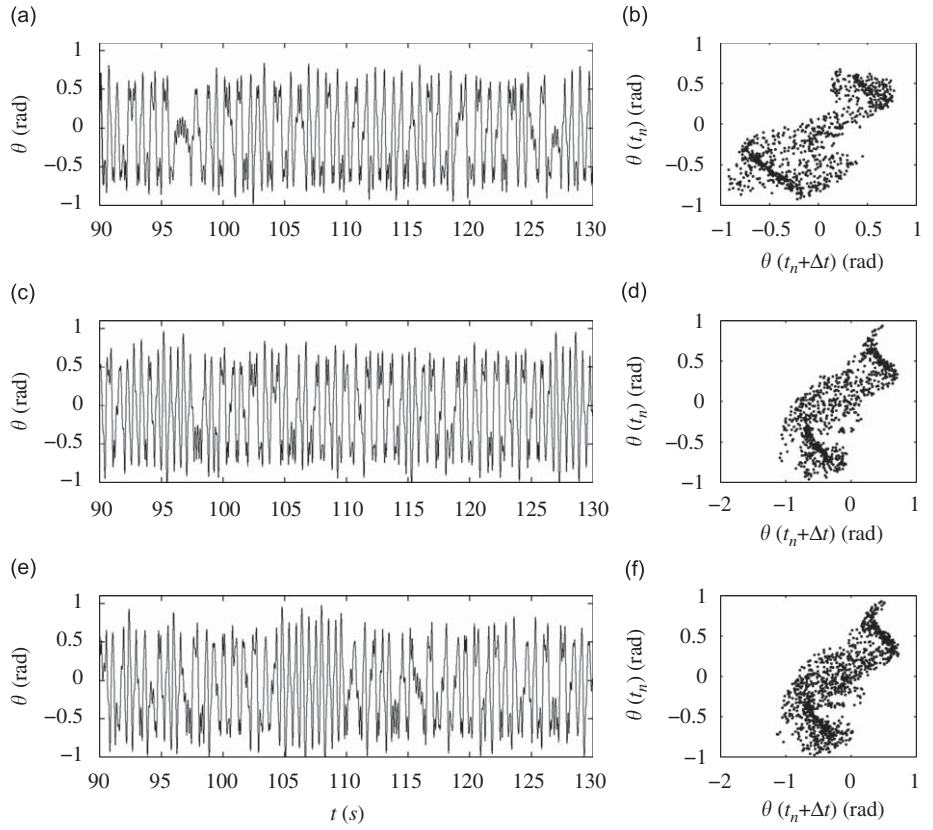

Fig. 10. Each row displays a 40 s time history and a Poincaré section of an experimental trial. Each result used a frequency of $\Omega = 10\pi$ rad/s and the following γ value: (a) and (b) are for $\gamma = 84.5\,(\mathrm{rad/s})^2$; (c) and (d) are for $\gamma = 86\,(\mathrm{rad/s})^2$; (e) and (f) are for $\gamma = 88\,(\mathrm{rad/s})^2$.

7. Summary and conclusions

This paper examines the nonlinear behavior of an experimental system. The magnetic pendulum system was experimentally characterized to determine the shape of the potential energy curve. Basins of attraction were computed to investigate the observed sensitivity to initial conditions (i.e. two closely spaced initial conditions may terminate in either potential well). Bifurcations of the unforced system were then studied when using the pendulum's mass as the control parameter.

A quasi-steady escape criterion from prior works was augmented to include the influence of parametric excitation and subharmonic response behavior. Furthermore, it was found that the parametric excitation term must be included in the calculation of $E_{\max}(\theta, \dot{\theta})$ to accurately estimate the instantaneous energy level. The procedure consists of determining the energy level that the system must obtain to overcome the local potential barrier and then using the predicted response amplitude and phase relationships to determine if an escape would occur. Since asymmetry exists in the potential energy curve, separate escape calculations were required—one for oscillations originating about each stable equilibria. The parametric excitation studies show a series of period-doubling cascades interrupted by a potential well escape—behavior that is correctly captured by the aforementioned threshold criterion. Finally, the escapes are shown to transition to chaotic motion at increased excitation amplitudes.

Acknowledgment

Support from a U.S. National Science Foundation CAREER Award is gratefully acknowledged.

References

[1] J.M.T. Thompson, Chaotic phenomena triggering the escape from a potential well, *Proceedings of the Royal Society of London A* 421 (1989) 195–225.

[2] J.A. Gottwald, L.N. Virgin, E.H. Dowell, Routes to escape from an energy well, *Journal of Sound and Vibration* 187 (1) (1995) 133–144.

[3] S.I. Lee, S.W. Howell, A. Raman, R. Reifenberger, Nonlinear dynamics of microcantilevers in tapping mode atomic force microscopy: a comparison between theory and experiment, *Physical Review B* 66 (115409) (2002) 1–10.

[4] S.I. Lee, S.W. Howell, A. Raman, R. Reifenberger, Nonlinear dynamic perspectives on dynamic force microscopy, *Ultramicroscopy* 97 (2003) 185–198.

[5] C. Pezeshki, E.H. Dowell, An examination of initial condition maps for the sinusoidally excited buckled beam modeled by Duffing's equation, *Journal of Sound and Vibration* 117 (2) (1987) 219–232.

[6] J. Guckenheimer, P.J. Holmes, *Nonlinear Oscillations, Dynamical Systems, and Bifurcations of Vector Fields*, Springer, New York, 1983.

[7] L.N. Virgin, R.H. Plaut, C.-C. Cheng, Prediction of escape from a potential well under harmonic excitation, *International Journal of Non-Linear Mechanics* 27 (3) (1992) 357–365.

[8] M.S. Soliman, J.M.T. Thompson, Global dynamics underlying sharp basin erosion in nonlinear driven oscillators, *Physical Review A* 45 (1992) 3425–3431.

[9] Y. Ueda, S. Yoshida, H.B. Stewart, J.M.T. Thompson, Basin explosions and escape phenomena in the twin well Duffing oscillator: compound global bifurcations organizing behaviour, *Philosophical Transactions of the Royal Society of London A* 332 (1990) 169–186.

[10] H.B. Stewart, Y. Ueda, Catastrophes with indeterminate outcome, *Proceedings of the Royal Society of London A* 432 (1991) 113–123.

[11] M.S. Soliman, J.M.T. Thompson, Indeterminant bifurcational phenomena in hardening systems, *Proceedings of the Royal Society of London A* 452 (1996) 487–494.

[12] M.S. Soliman, J.M.T. Thompson, Indeterminant sub-critical bifurcations in parametric resonance, *Proceedings of the Royal Society of London A* 438 (1992) 511–517.

[13] V.A. Yakubovich, V.M. Starzhinskii, *Linear Differential Equations with Periodic Coefficients*, Wiley, New York, 1975.

[14] K.G. Lindh, P.W. Likins, Infinite determinant methods for stability analysis of periodic-coefficient differential equations, *AIAA Journal* 8 (1970) 680–686.

[15] A.H. Nayfeh, D.T. Mook, *Nonlinear Oscillations*, Wiley, New York, 1979.

[16] D.A. Peters, K.H. Hohenemser, Application of Floquet transition matrix to problems of lifting rotor stability, *Journal of the American Helicopter Society* 16 (1971) 25–33.

[17] C.S. Hsu, W.H. Cheng, Application of the theory of impulsive parametric excitation and new treatment of general parametric excitation problems, *Journal of Applied Mechanics* 40 (1973) 78–86.

[18] G.H. Gaonkar, D.S.S. Prasad, D. Sastry, On computing Floquet transition matrices of rotorcraft, *Journal of American Helicopter Society* 26 (1981) 56–61.

[19] S.C. Sinha, R. Pandiyan, J.S. Bibb, Liapunov–Floquet transformation: computation and applications to periodic systems, *Journal of Vibration and Acoustics* 118 (1996) 209–219.

[20] S.C. Sinha, C.C. Chou, H.H. Densinha, Stability analysis of systems with periodic coefficients: an approximate approach, *Journal of Sound and Vibration* 64 (1979) 515–527.

[21] S.C. Sinha, D.H. Wu, An efficient computational scheme for analysis of periodic systems, *Journal of Sound and Vibration* 151 (1) (1991) 91–117.

[22] N.K. Garg, B.P. Mann, N.H. Kim, M.H. Kurdi, Stability of a time-delayed system with parametric excitation, *Journal of Dynamic Systems Measurement and Control* 129 (2007) 125–135.

[23] D. Haliday, R. Resnick, *Fundamentals of Physics*, third ed., Wiley, New York, NY, 1988.

[24] B.P. Mann, M.A. Koplow, Symmetry breaking bifurcations of a parametrically excited pendulum, *Nonlinear Dynamics* 46 (4) (2006) 427–437.

[25] B.P. Mann, F.A. Khasawneh, An energy balance approach for oscillator parameter identification, *Journal of Sound and Vibration* 321 (2009) 65–78.

[26] C.D. Boor, *A Practical Guide to Splines*, Springer, New York, NY, 1978.

[27] E. Kreyszig, *Advanced Engineering Mathematics*, eighth ed., Wiley, New York, NY, 1999.

[28] H.D.I. Abarbanel, *Analysis of Observed Chaotic Data*, second ed., Springer, New York, 1996.